Journal of Polymer Research (2024) 31:223
https://doi.org/10.1007/s10965-024-04066-5

ORIGINAL PAPER

Impact of graphene nanoplatelet size and hybridisation on the properties of natural rubber nanocomposites

Wichain Chailad[1] · Phornwalan Nanthananon[1] · Waroonsiri Jakarbutr[1] · Nichanan Phansroy[1] · Suchalinee Mathurosemontri[1]

Received: 17 April 2024 / Accepted: 3 July 2024 / Published online: 12 July 2024

Abstract

This study explores how the size and hybridisation of graphene nanoplatelets (GNPs) affect the properties of graphene nanoplatelet-filled natural rubber (NR) nanocomposites (GNP-filled NR). Results demonstrate notable enhancements in the thermal properties and electrical conductivity of NR with the addition of GNPs. However, mechanical properties experienced partial enhancement, showing increased modulus by up to 200% and hardness by up to 50%, alongside decreased tensile strength by up to 60% and elongation by up to 70%. The comparative analysis highlights the superior mechanical and thermal properties associated with smaller GNPs. These smaller particles enhanced mechanical properties such as modulus at 100% strain and Shore A hardness, increased the glass transition temperature by up to 10%, and reduced thermal degradation rates by up to 30% due to their superior dispersion and interfacial bonding with NR. Larger GNPs exhibited a 1000% increase in electrical conductivity at 10×10^6 Hz due to increased surface area and network formation due to reduced dispersion. Notably, hybrid GNPs contributed significantly to overall property enhancements compared to the single filler system, with up to 80% higher tensile strength, up to 30% higher elongation at break, up to 20% higher glass transition temperature, lower degradation rate at high temperature, attributed to improved dispersion of GNPs and interfacial adhesion with NR. This study highlights the substantial influence of GNP sizes on the performance of NR nanocomposites and the significant effects of hybridisation, providing valuable insights for optimising material properties for advanced applications.

Keywords Graphene nanoplatelets (GNP) · Natural rubber (NR) · GNP-filled NR nanocomposites · Physical and mechanical properties · GNP sizes and hybridisation

Highlights

- Smaller graphene nanoplatelet (GNP) sizes yield superior mechanical and thermal properties by enhancing dispersion and interfacial bonding with natural rubber (NR).
- Smaller GNP sizes enhance thermal stability in graphene nanoplatelet-filled natural rubber nanocomposites (GNP-filled NR), reducing degradation rates.
- Larger GNP sizes enhance electrical conductivity through increased surface area and network formation due to reduced dispersion.
- Hybrid GNP-filled NR outperforms single GNP-filled NR in mechanical and thermal properties due to improved dispersion and efficient stress transfer, although with lower electrical conductivity.

✉ Wichain Chailad
wichain_c@rmutt.ac.th

✉ Suchalinee Mathurosemontri
suchalinee.m@en.rmutt.ac.th

[1] Department of Materials and Metallurgical Engineering, Faculty of Engineering, Rajamangala University of Technology Thanyaburi, Pathum Thani 12110, Thailand

Introduction

Natural rubber (NR), derived from Hevea Brasiliense's trees, comprises 93–95% cis 1, 4-polyisoprene and is prized for its exceptional physical properties such as elasticity, resilience, and abrasion resistance. However, its susceptibility to heat, ozone, and chemicals and poor compatibility with other materials restrict its industrial applications. Active fillers and polymer modifications are necessary to overcome these limitations, enhancing properties while retaining their inherent advantages [1]. Polymer composites, incorporating NR with reinforcing fillers, significantly improve mechanical, physical, chemical, and electrical properties, enhancing processability and reducing costs. Traditional fillers like carbon black (CB), silica, and clay have been extensively used, but they often require high loading levels, compromising processability and resulting in brittleness [2–4]. In recent years, integrating advanced nanomaterials into polymer

matrices has emerged as a promising avenue for enhancing the mechanical, physical, thermal, and electrical properties of polymers [5–8]. Among the many nanofillers, graphene nanoplates (GNP) have gained significant attention due to their exceptional mechanical strength, thermal conductivity, and electrical conductivity [9–11].

In recent years, there has been a surge of interest in the remarkable properties of 2D materials, particularly graphene and its derivatives [5–7]. Graphene demonstrates exceptional mechanical properties, with an elasticity modulus of around 1 TPa and an unparalleled strength of around 130 GPa. It also offers high thermal conductivity as high as 5000 W/mK, a large specific surface area, remarkable electrical conductivity, and significant gas permeability [12, 13]. Given these properties, it is unsurprising that graphene-based particles are extensively studied as nanofillers in polymer and elastomer matrices to enhance their properties. For instance, graphene nanoplatelets (GNPs) have been shown to significantly improve the overall physical and mechanical properties of polymers, even in small amounts, while preserving their inherent advantages [3, 9–11, 14]. Studies by Li et al. [3] showed that GNPs could enhance the stiffness of NR up to three times more than N330 CB for the same filler amount. Similarly, research by Young et al. [9] showed that incorporating GNPs into an epoxy matrix increased its thermal conductivity by 23 times with just a 10% volume loading. Wijerathne et al. [14] observed that introducing small amounts of GNP in recycled polycarbonate could improve Young's modulus by around 40% and its thermal stability of 2.74%.

The synergistic combination of natural rubber (NR) with graphene nanoplatelets (GNPs) holds immense potential for developing high-performance nanocomposites, offering a unique blend of mechanical robustness and flexibility. This study investigates the influence of GNP sizes on the properties of GNP-filled NR. The size of GNPs is a critical parameter that can significantly impact the interaction between the GNP particles and the NR matrix, thereby influencing the overall performance of the GNP-filled NR. As researchers strive to tailor the properties of these materials for diverse applications, a thorough understanding of the size-dependent effects of GNP on the mechanical, thermal, and electrical characteristics of GNP-filled NR becomes imperative.

This research uniquely explores the impact of varying GNP sizes on the thermal, mechanical, and electrical properties of GNP-filled NR, providing detailed insights into how different sizes of GNPs affect these properties. Additionally, it introduces and evaluates hybrid GNP systems, combining multiple sizes to understand their synergistic effects on the properties of the obtained hybrid GNP-filled NR —an area not extensively covered in previous studies. The research offers a comprehensive analysis of property enhancements, considering trade-offs such as increased modulus versus decreased tensile strength and elongation, providing an understanding of material behavior. This research aims to enhance the performance of NR by examining how GNP size and hybridisation affect GNP-filled NR, optimising properties for specific applications where improved mechanical, thermal and electrical properties are crucial.

Given the industrial relevance of NR, improving its performance through advanced nanocomposite techniques can lead to significant benefits, including better durability and functionality of NR products. By addressing the knowledge gap in the detailed comparison of different GNP sizes and hybrid systems on NR nanocomposites, this research seeks to fill these gaps and provide a foundation for future work. The outcomes of this research contribute to the growing body of knowledge in the field of polymer nanocomposites, paving the way for developing advanced materials with enhanced multifunctionality.

Materials and method

Materials

The XG graphene nanoplatets (GNPs) were obtained from XG Sciences Inc., East Lansing, MI, United States. GNP was utilised without additional modification. Three different GNP grades, designated as G5, G15, and G25, with nominal lateral diameters of 5 µm, 15 µm, and 25 µm, respectively, were employed in this study. According to the manufacturer, the thickness of all flakes ranges between 6–8 nm, equating to approximately 20 layers of graphene [15–17]. The GNPs consist of 95–100% graphite and 1–5% elemental sulfur. The main properties of these GNPs are detailed in Table 1.

Table 1 Characteristics of different types of GNPs [15–17]

GNP types	Density (g/cm^3)	Bulk Density (kg/m^3)	Lateral diameter (µm)	Aspect ratio (D/L)	Specific Surface area (m^2/g)	Electrical Conductivity (S/cm)	Thickness (nm)	Number of layers
G5	2.2	160	5	215.5	150	34	6–8	15–20
G15	2.2	66	15	N/A	120–150	35	6–8	15–20
G25	2.2	67	25	1116.1	120	22	6–8	15–20

The grade of NR (cis 1,4 poly isoprene) utilised in this study was Standard Malaysian Rubber 60 (SMR60), which has the Mooney-Viscosity ML (1 + 4, 100 °C) of 60. SMR60 was sourced from Thai Hua Rubber Company and employed in its original state without further modification. All additives utilised in the processing of the NR and GNP-filled NR compounds, including stearic acid, zinc oxide (ZnO), sulfur, and N-Cyclohexyl-2-benzothiazole sulfenamide (CBS) accelerator, were of analytical grade and employed without further modification.

Methods

Preparation of GNP-filled NR

A mini-internal mixer operating in the Banbury mixer mode, manufactured by Thermo Scientific, was employed to masticate the NR. This process followed the formulations detailed in Table 2. Three different types of GNPs (G5, G15 and G25) were incorporated into the NR matrix at nominal loadings to prepare GNP-filled NR. Furthermore, three hybrid samples of GNP-filled NR were created by blending two different GNP grades, as specified in Table 2.

The pieces of NR were initially cut into suitable sizes and then pre-heated at 60 °C for approximately 30 min to facilitate decrystallisation. This step was crucial for preparing the material for further processing, ensuring optimal properties in the final GNP-filled NR. Once warm and sticky, the NR was mixed using a mini-internal mixer. ZnO, stearic acid, and CBS accelerator were then added and mixed at the proper time. GNPs were gradually incorporated into the compound, with mixing time adjusted based on the number of additives. The final step involved the addition of sulfur, which was carefully mixed into the NR compound.

Further mixing was conducted to ensure the uniform dispersion of all additives and GNPs within the NR matrix. Mixing time and temperature were carefully controlled and kept below 100 °C to prevent premature vulcanisation. Torque observation helped control additive addition and ensured sufficient mixing. The 60 g portions of NR compounds were cut and then compressed in a mould with the dimensions of 148 × 148 × 2.5 mm (length x width x thickness), utilising a Collin press P300 P/M. The NR compounds were subjected to vulcanisation at 160 °C for 10 min, applying a hydraulic line pressure of 30 bar. The preparation steps are shown in Fig. 1.

Characterisation techniques

Raman spectroscopy Raman spectra of the NR and different GNPs were collected over a Raman shift range of 100–3000 cm^{-1} using a Renishaw 200 Raman spectrometer equipped with a laser wavelength of 633 nm and an ×50 objective lens, providing a spot size of approximately two µm. GNP particles were identified from small clusters deposited on glass slides. Laser power was varied from 10% to 50%, and each spectrum was acquired with an exposure time of 50 s.

Scanning electron microscopy A QUANTA FEG 650 microscope operating between 8 and 10 kV was used to conduct the Scanning electron microscopy (SEM) analysis. The particles of GNP were dispersed onto aluminium stubs before the analysis. The microstructures of GNP-filled NR samples were analysed from surfaces which were fractured at low-temperature. First, the GNP-filled NR specimens were submerged in liquid nitrogen and manually fractured to generate distinct brittle fracture surfaces. Subsequently, the fracture surfaces of the GNP-filled NR samples underwent treatment

Table 2 GNP-filled NR compound formulation

Raw materials	Amount (phr [a])			
SMR CV60	100			
ZnO	3			
CBS accelerator	1			
Sulphur	3			
Stearic acid	2.5			
Samples	GNP types			Symbols
	G5	G15	G25	
1	20			G5
2		20		G15
3			20	G25
4	10	10		G5/G15
5	10		10	G5/G25
6		10	10	G15/G25

[a]phr denotes parts per hundred rubber

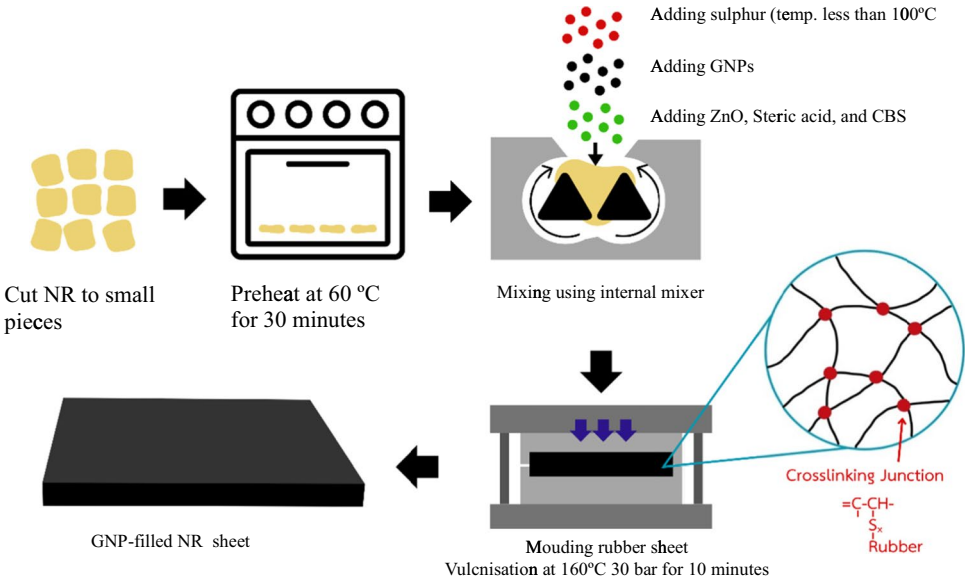

Fig. 1 The preparation process of GNP-filled NR

with an alloy of Au/Pd to guarantee conductivity prior to SEM analysis. This approach facilitated a comprehensive examination of the morphology and dispersion of GNPs within the NR matrix, offering valuable insights into the structure of the GNP-filled NR.

X-ray diffraction X-ray diffraction (XRD) analysis was conducted to examine the structural characteristics of different GNPs. Rectangular specimens measuring 20 mm × 20 mm × 2.5 mm were prepared for analysis. Using a Proto AXRD θ-2θ diffractometer, XRD measurements were performed. The diffractometer was supplied with a filtered Cu-Kα radiation source with a wavelength of 0.1542 nm. The equipment operated at a current of 40 mA and a voltage of 40 kV. Data collection was carried out in the 2–50 2Θ range using a Dectris Mythen 1 K 1D detector, which has a 3.22° maximum active length. The results are applied to examine the crystallographic structure of the GNP-filled NR samples.

Tensile testing Tensile testing was performed using an Instron-5969 universal testing machine. The specimens were prepared by cutting the NR compound sheets into using a standard die type C for cutting a dumbbell shape having a gauge size of 33 mm in length and 6 mm in width. To mitigate the effects of moisture on NR specimens, they were conditioned for 24 h, according to ADTM D412. Testing was conducted on each formulation with five specimens until fracture occurred, using a crosshead speed of 500 ± 50 mm/min. Initially, strain measurements were tracked using video tracking. Additionally, changes in grip at higher elongation levels were also observed.

Hardness testing A Shore A durometer (RS Pro Durometer) was used to test the hardness of NR compounds following ASTM D2240 standards. The durometer was positioned vertically, ensuring the indenter point was at least 12 mm from the edge of the specimens. The specimens were quickly subjected to the pressure foot. Five specimens from each sample were evaluated, and testing was conducted at a temperature of 23 ± 2°C. This method allowed for precise measurement of the resistance of material to indentation, providing valuable insights into its mechanical properties.

Dynamic mechanical analysis Dynamic mechanical analysis (DMA) was conducted using a TA Instruments DMA Q800 in dual-cantilever mode. Rectangular sample sizes of 35 mm × 10 mm × 2.5 mm were used for testing. Testing temperatures ranged from -80 °C to 100 °C under a nitrogen environment, with a heating rate of 3 °C/min. The DMA was operated at a frequency of 1 Hz and 50 µm strain amplitude. This comprehensive approach allowed for detailed characterisation of the dynamic of material mechanical properties over a wide temperature range, which provided valuable insights into its thermal behaviour and viscoelastic properties.

Differential scanning calorimetry Differential scanning calorimetry (DSC) (TA Instruments Q100 DSC) was used to investigate the thermal behaviour of the unfilled and GNP-filled NR samples. Under a nitrogen atmosphere (N2), the temperature was ramped from -100 °C to 300 °C at a heating rate of 10°C/min. Approximately 10 mg of each NR compound underwent heating–cooling-heating cycles to assess the impact of GNPs on the thermal properties of the

GNP-filled NR. By observing the initial change in the heat capacity curve during the second heating cycle, the glass transition temperature (Tg) was determined.

Thermogravimetric analysis The thermal behaviour of the unfilled and GNP-filled NR samples was assessed using a TA Instruments Q500 Thermogravimetric analysis (TGA), which also provided the actual fraction of GNP volumes within the samples. The temperature was ramped up at 40 °C/min heating rate from ambient conditions to 800 °C in N_2. The quantity of other additives was assumed to remain consistent in the pure NR to assess the mass proportion of GNP in the GNP-filled NR. The mass ratio will be transformed into the volume ratio using Eq. (1) and (2).

$$V_i = \frac{\rho_c}{\rho_i} W_i \tag{1}$$

$$\rho_c = \frac{1}{\sum_{i=1}^{n} (W_i/\rho_i)} \tag{2}$$

where the density of the GNP-filled NR is denoted by ρ_c and ρ_i stands for the density of component i. W_i donates a portion of component i by mass. V_i presents a portion of component i by volume. Two specimens of each sample were examined.

Electrical conductivity The rectangular test specimens were carefully extracted from the broader top and bottom edges of the cutting die to ensure consistency. Their dimensions were accurately gauged and documented for subsequent examination. These samples underwent electrical conductivity testing through a two-electrode approach. To enhance conductivity, silver conductive epoxy was used on each surface of the specimens, allowed to be set for 30 min, and then cured at 120 °C. The curing time was 10 min. Copper wires were then connected sequentially to complete the setup.

An electrochemical impedance spectroscopy (EIS) was used to analyse the resistance of the unfilled and GNP-filled NR samples. The model used EIS was a Numeric Q phase-sensitive multi-meter (PSM 1735). A frequency between 1 and 10^6 Hz was used. The conductivity values of each specimen were determined three times to ensure accuracy. Electrical conductivity, expressed in S/m, was calculated using Eq. (3) based on the resistance values and sample dimensions according to ASTM D4496.

$$\sigma(S/m) = \frac{1}{R_A} x \frac{t}{A_s} \tag{3}$$

where R_A is measured resistance (Ω), t is specimen thickness (m), and A_s is the effective area of the measuring electrode (m^2).

Results and discussion

Characterisation of GNPs

Raman spectroscopy

The results from Raman spectroscopy for the unfilled NR and three different grades of GNPs are presented in Fig. 2 and Table 3. The Raman spectra for all GNP sizes displayed strong D, G, and 2D bands, demonstrating the presence of a graphitic structure in the materials [3, 18]. In contrast, the Raman band of NR exhibited solely a broad peak attributed to a fluorescent background originating from the NR matrix.

Figure 2 and Table 3 illustrate that all GNP types exhibit a G-band peak, found at around 1581.9 cm^{-1}, suggesting the vibration mode of sp^2 hybridised carbon atoms in a two-dimensional hexagonal lattice [20, 21]. Using Eq. (4),

$$\omega_G = 1581.6 + \frac{11}{(1 + n^{1.6})} \tag{4}$$

where w_G represents the wavelength position of the G band, while n denotes the number of graphene layer thicknesses and based on the G-band position, the number of graphene layers in GNPs was calculated, revealing a consistent average of approximately 11 ± 2 layers across all GNP types despite variations from G5 to G25.

The presence of the D band in Raman spectra signifies defects or disorders in graphene-based materials, typically associated with amorphous carbon types, vacancies, grain boundaries, and heteroatoms [21, 22]. The I_D/I_G ratio, used to compare defect levels in GNPs, revealed the highest defect density on smaller GNPs (G5) surfaces, indicated by a higher I_D/I_G ratio compared to G15 and G25. These defects are attributed to the increase in the percentage of dangling bonds and oxidation degree in smaller particles, particularly in G5 [23]. While Raman spectra for hybrid GNPs were not

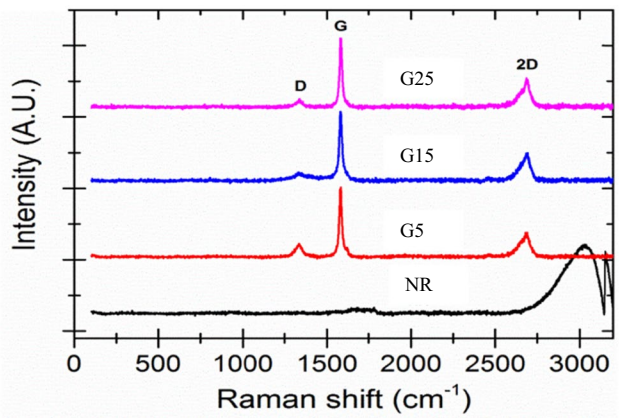

Fig. 2 The Raman spectra of NR and different GNP types

Table 3 The positions of the main peaks in the Raman spectra from the various GNPs utilised in this study

GNP types/ Characteristics	Raman Shift		Peak Intensity		I_D/I_G	Calculated number of layers	Calculated thickness [a]
	Band Position (cm^{-1})		Band				
	D	G	D	G		(layers)	(nm)
G5	1336.22	1581.93	368.30	1984.81	0.186	9	3.0
G15	1336.22	1581.83	178.44	1431.48	0.125	11	3.7
G25	1338.40	1581.78	151.44	1280.21	0.118	13	4.4

[a]To determine the thickness of each GNP type, the number of graphene layers was converted using a single graphene layer thickness of 0.335 nm. [19]

acquired in this investigation, it is expected that the results would integrate characteristics observed in individual GNP types. This integration may potentially present distinct properties advantageous for composite materials.

Scanning *electron* microscopy

The results in Fig. 3(a)–(c) present the SEM images of hybrid GNPs. The platelet-like structure of GNPs is clearly visible. The SEM micrographs of hybrid GNPs with different sizes show distinct distances between various-sized GNP plates, resulting in less agglomeration—a phenomenon rarely observed in single GNP systems, as reported in other studies [3] and Fig. 4(a). The increased separation between GNP particles in hybrid systems suggests fewer interparticle contacts, indicating that GNPs in hybrid systems may disperse more effectively during mixing processes compared to single GNPs. Consequently, hybrid GNPs are anticipated to exhibit better dispersion at the same filler loading.

Figure 4 compares the SEM micrographs of GNP platelets and GNP-filled NR. The SEM images of the G5 (Fig. 4(a)) reveal the characteristic platelet-like structure of the GNP with a nominal lateral diameter of 5 µm. The individual G5 platelets exhibit a high degree of flatness and sharp edges, indicative of their well-defined layered structure. In contrast, the SEM image of the G5-filled NR (Fig. 4(b)) displays a distinctly different microstructure. The G5 particles were embedded within the NR matrix, and their dispersion and distribution can be clearly observed. G5 appeared to be more evenly distributed in the NR with minimal agglomeration. The smaller particle size facilitates a more homogeneous dispersion throughout the NR matrix, which would increase its effectiveness as a reinforcing filler.

X-ray diffraction

The purity and crystalline structure of the GNPs were validated using XRD analysis. Figure 5 summarises the findings, where strong peaks corresponding to (002) were observed for all GNPs at $2\Theta \sim 26.6°$, closely matching the graphite bulk typically at $2\Theta \sim 27°$ [24]. The differences in peak intensity (height) between the GNP-filled NR samples are negligible and are affected by sample quantity and preparation. The distinct (002) peaks further confirm the crystallinity of the GNPs. The full width at half maximum (FWHM) values for all GNPs are below 6.25×10^{-3} rad. G5 exhibits the highest FWHM among them, indicating greater stacking defects and disorder in its crystal structure [24].

The interlayer distance between graphene layers, known as d-spacing, was determined using HighScorePlus software and found to be approximately 0.33 nm for all GNPs. The calculated results are shown in Table 4. This finding aligns with previous studies by Um et al. [17] and Chong et al. [24], which stated that d-spacing values ranged from 0.33 to 0.34 nm for GNPs. The NR matrix exhibited typical characteristics of an amorphous polymer in its XRD pattern, showing a broad peak centred at approximately $2\theta \sim 18°$. Moreover, in the range of $2\theta \sim 30°$-$40°$, distinct diffraction peaks were observed, attributed to the occurrence of ZnO particles within the vulcanised NR matrix [25]. Crystal sizes were determined using the Scherrer equation (Eq. (5)) [26].

$$\text{Crystallite size (L)} = \frac{k * \lambda}{\text{FWHMxcos}0} \quad (5)$$

A shape constant k of 0.9, diffraction angle θ of the peak, the wavelength of the radiation λ, and FWHM in radians were employed to derive the average crystallite size of

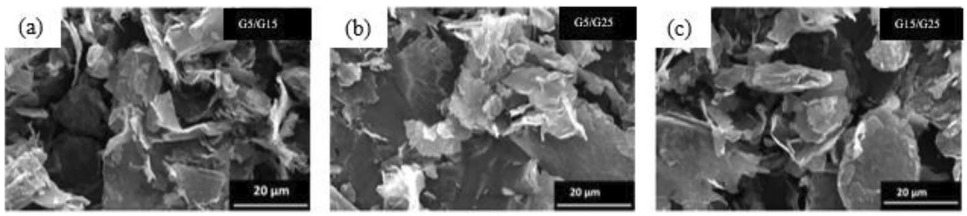

Fig. 3 SEM images of GNP: hybrid mixtures of (**a**) G5/G15, (**b**) G5/G25, and (**c**) G15/G25

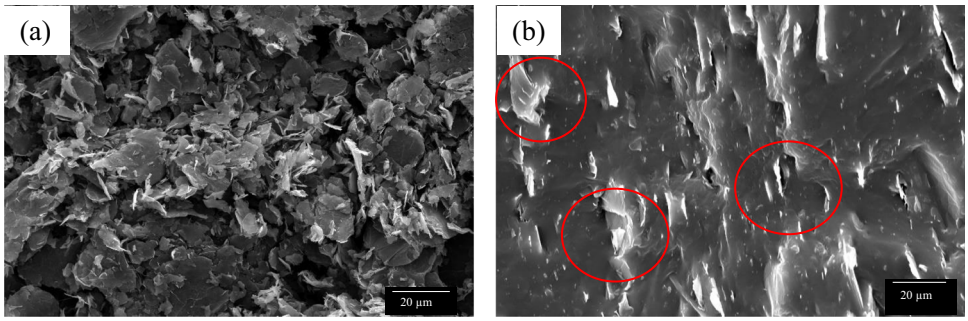

Fig. 4 SEM image of G5 (**a**) and fracture surfaces of G5-filled NR nanocomposites (**b**)

GNPs, which can be found in Table 4. The broader (002) peaks indicate a reduction in graphene layer thickness in GNPs [21]. Consequently, the GNP with the highest FWHM, G5, exhibited the smallest crystal size, inversely proportional to its thickness. The calculated aspect ratios of the GNPs stated in Table 4 were found to be proportional to their diameters, with G25 exhibiting the highest aspect ratio due to its larger lateral diameter, consistent with findings in previous research [16, 17, 27, 28].

However, the calculated aspect ratio values for all GNP sizes were lower than those provided by the manufacturer, possibly due to variations in the thickness values obtained from XRD. Interestingly, the number of graphene layers obtained from XRD was higher than that obtained from Raman spectroscopy, indicating a potential difference in techniques. Nevertheless, both techniques yielded consistent trends, with G25 exhibiting the highest graphene thickness among the three GNP types. Although hybrid GNPs were not subjected to XRD analysis in this study, it is anticipated that the outcomes would reflect a combination of those observed for individual GNP types in the hybrid system.

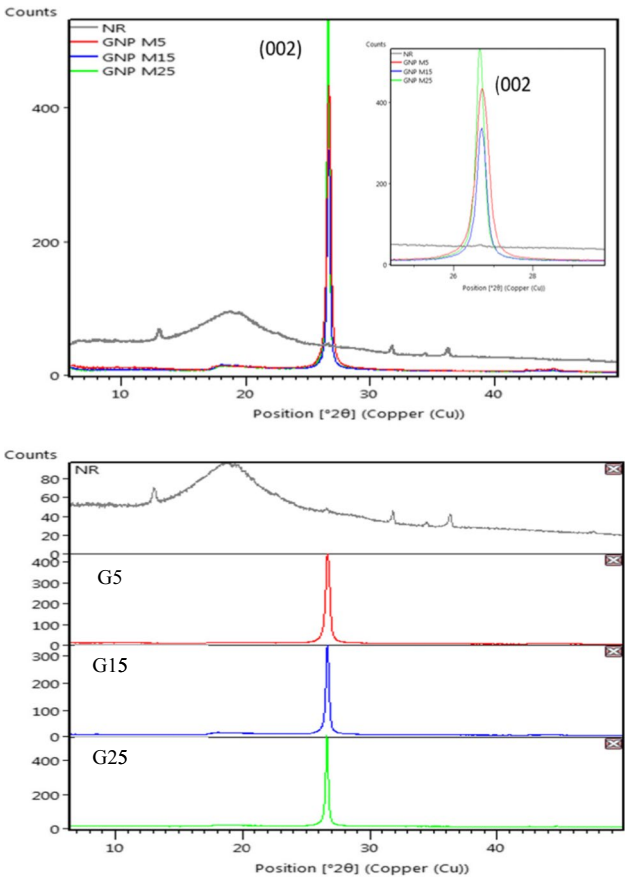

Fig. 5 XRD patterns of NR and GNPs used in this study

Table 5 presents a comparative analysis of the characterised results obtained from the manufacturer's specifications, Raman spectroscopy, and XRD for the three GNP sizes. In this study, the high specific surface area of the smallest particulate fillers, G5, can be attributed to the reduction in primary particle diameter, which leads to decreased aggregate size and inter-aggregate distance, thereby increasing the surface area [29]. G5 exhibits the highest specific surface area, degree of defects in its structure, and bulk density alongside the smallest graphene thickness and lateral diameter. The greater bulk density facilitates improved dispersion of G5 particles within the NR matrix, leading to a more pronounced dispersion level than larger GNP, G15 and G25 [17]. The increased specific surface area enhances contact between G5 and the NR matrix, facilitating a more pronounced filler network formation. Higher defects and a rough topology also accelerate crosslinking reactions [23].

Despite its greater thickness, G25 maintains the maximum aspect ratio because of its larger diameter, enhancing contact areas and promoting stress transfer from the matrix. However, the higher graphene thickness and larger lateral diameter in G25 may lead to filler stratification, resulting in inhomogeneous composite materials and potentially anisotropic behaviour.

Although the greater graphene thickness and larger lateral diameter in G25 may contribute to filler stratification, it could result in inhomogeneous composite materials and potentially anisotropic behaviour. Regarding viscosity, decreasing the particle size while maintaining the weight of fillers increases the number of particles in the system, enhancing NR-particle interactions and viscosity. This can lead to higher resistance to flow, indicating immobility and hydrodynamic effects of the filler in unvulcanised NR.

Table 4 The peak positions of FWHM and 2Θ of GNPs obtained by XRD

GNP types/ Characteristics	d-Spacing (nm)	2Θ Peak Position	FWHM (Rad, $\times 10^{-3}$)	Number of graphene layers (layers)	Average crystallite size (nm)	Aspect ratio (D/L)
G5	0.3333	26.6928	6.25	74	24.83	202
G15	0.3339	26.6741	4.57	101	34.01	442
G25	0.3344	26.6357	3.71	125	41.86	596

Therefore, due to its larger size and weight, the low viscosity and stratification observed in G25 could result in inferior performance of G25-filled NR. Analysis comparing single and hybrid GNP-filled NR systems based on SEM data indicates that GNP platelets in hybrid systems may achieve better dispersion due to their varied sizes and more considerable inter-particle distances, thereby lowering the chances of agglomeration.

Characterisation of GNP-filled NR

Mechanical properties

Stress–strain behaviour Figure 6 shows the tensile results of unfilled and GNP-filled NR samples. The unfilled and GNP-filled NR samples showed a typical nonlinear elastic behaviour consistent with amorphous, crosslinked polymers at temperatures below T_g. The tensile stress gradually increased with increasing tensile strain, followed by a sharp increase as the strain approached 600%, which was attributed to strain-induced crystallisation [3, 30–32]. Similar stress–strain behaviour was observed in NR reinforced by single and hybrid GNPs systems. Figure 6(a) illustrates the comparative results of all samples, indicating a significant increase in tensile stress with the addition of GNPs. Notably, the mechanical property enhancement was more pronounced in NR nanocomposites filled with smaller sizes and hybrid systems. This effect is particularly evident at 300% strain, as shown in Fig. 6(b), a crucial indicator for practical applications.

Comparing the stress–strain curves between the unfilled and GNP-filled NR samples, upon examination, it is evident that the GNP-filled NR samples exhibit a notable increase in tensile stress, initiating at significantly lower strain levels compared to the unfilled NR, with approximately 300% strain observed across all samples. These findings underscore the significant influence of GNPs on the strain-induced crystallisation behaviour of NR, primarily owing to their robust and durable interfacial interaction with the NR matrix. Incorporating GNPs changed the stress distribution, amplifying the strain in the polymer chains locally and triggering strain-induced crystallisation at lower strain levels during stretching, a phenomenon referred to as strain amplification [33].

In general, the initial slopes of the stress–strain curves for GNP-filled NR samples, known as modulus, demonstrated an increase with the incorporation of GNPs, highlighting their role in reinforcing the NR matrix. In GNP-filled NR, tensile strength showed a remarkable decrease of up to 60% when reinforced with single GNPs, particularly evident in the largest size (G25), whereas those reinforced with hybrid GNPs showed relatively minor changes. Additionally, elongation at break reduced across all samples, with significant decreases observed in single GNP-filled NR, notably in the smallest size (G5). The elongation at the break of unfilled NR decreased up to 70% after adding GNPs.

Figure 7 demonstrates that incorporating GNPs as reinforcing fillers led to significantly steeper initial slopes in the stress–strain curves, indicating that the modulus at least doubled compared to unfilled NR. The stress at 300% of unfilled NR increased to 200% after adding GNPs. This increase in tensile modulus was observed across all samples upon the addition of GNPs, whether using single or hybrid fillers. The enhancement in tensile moduli can be attributed to several factors: Firstly, GNPs possess outstanding mechanical properties and higher specific surface areas. Secondly, the irregularity and surface defects of GNPs establish a rough and wrinkled nanoscale texture, promoting robust interactions between GNP and NR, thereby enhancing the mechanical properties of GNP-filled NR. Lastly, NR molecular

Table 5 Characterisation of GNPs by manufacturer*, Raman spectroscopy, and XRD

Properties/ GNP types	G5	G15	G25
Number of particles per unit weight*	H[a]	M[a]	L[a]
Bulk density*	H	M	L
Specific surface area*	H	M	L
Graphene thickness	L	M	H
Lateral diameter	L	M	H
FWHM	H	M	L
Aspect ratio	L	M	H
I_D/I_G	H	M	L

[a]H stands for highest, M is medium, and L is lowest

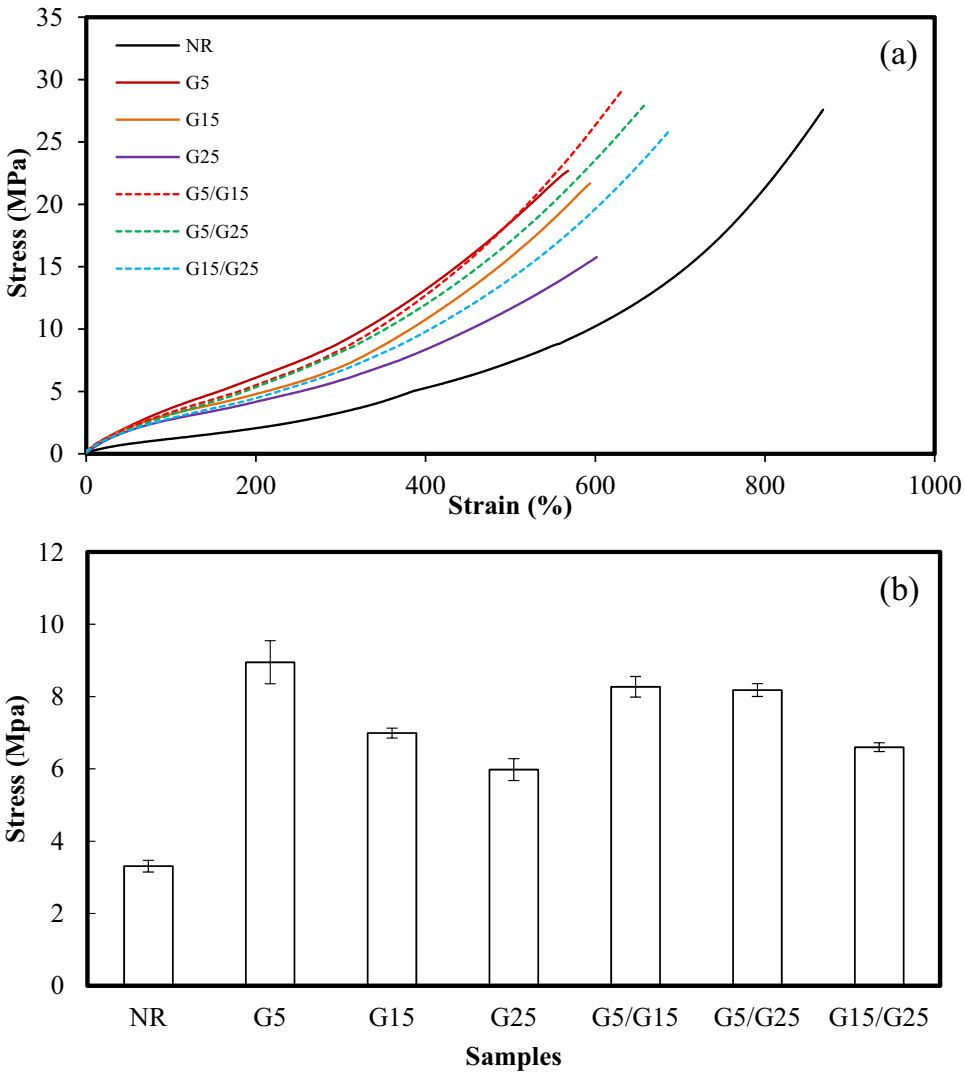

Fig. 6 Uniaxial tensile stress–strain curves stress–strain curves for the unfilled and GNP-filled NR (**a**) and Stress measurement at 300% strain (**b**)

chains-GNP interactions may provide additional physical crosslinking or entanglements.

Table 6 demonstrates that the G5, which has the smallest lateral diameter, had the most significant impact on enhancing the tensile modulus of GNP-filled NR compared to other GNPs. For example, incorporating G5, G15, and G25 resulted in approximately 200%, 160%, and 140% enhancements in the tensile modulus of their respective GNP-filled NR compared to unfilled NR. Despite adding all three GNPs at the same amount, the particles differed significantly. Based on manufacturer data in Table 5, it is apparent that G5 had the highest specific surface area, while G25 had the lowest. More particles per unit weight mean more contact areas, facilitating increased surface interaction between NR and GNP and a greater modulus enhancement.

Furthermore, the findings from Raman spectroscopy highlighted that G5 exhibited the most pronounced surface defects, which facilitated enhanced interfacial bonding between GNPs and the NR matrix. As expected, in the hybrid GNP system, the tensile modulus values of NR reinforced with hybrid GNPs were found to lie between those of the NR nanocomposites reinforced with the respective single GNP types. Notably, NR reinforced with hybrid G5 and G15 (G5/G15) demonstrated the highest modulus among the other hybrid GNP-filled NR samples, attributed to more GNP particles than hybrid G5/G25 and G15/G25 as the modulus is directly influenced by the amount of contact area between the fillers and the matrix.

The modulus values at 100% strain for GNP-filled NR were compared to NR filled with alternative fillers at similar content found in the literature, as illustrated in Table 7. Evidently, the moduli at 100% strain of GNP-filled NR surpassed those of other fillers at comparable loadings, exhibiting significantly higher modulus at 100% strain values of over 200%, particularly for G5-filled NR. These findings underscore the advantageous characteristics of employing GNP as fillers in NR compounds.

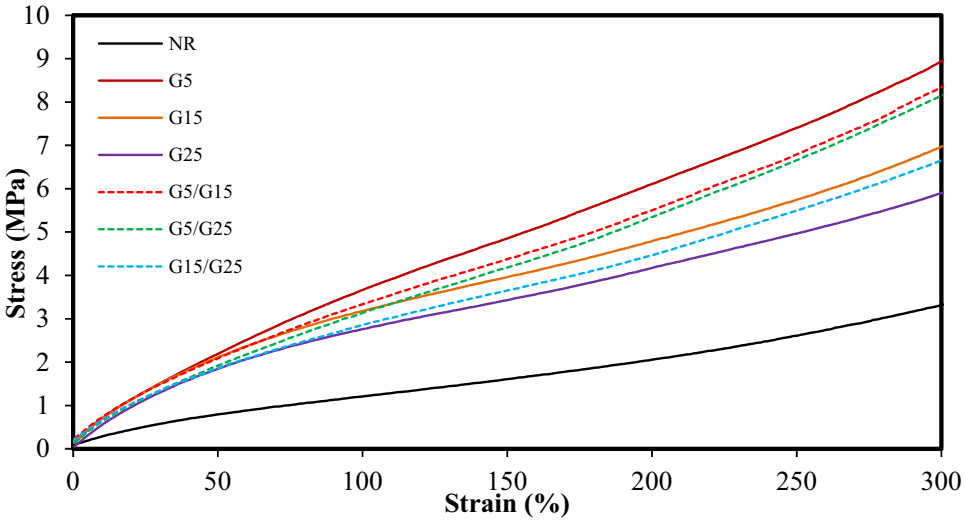

Fig. 7 Uniaxial tensile stress–strain behaviours of the unfilled and GNP-filled NR measured until 300% strain

Prediction of the theoretical *modulus* of GNP-filled NR Using the rule of mixture model, the effective moduli (E_f) of GNP-filled NR with different sizes of GNPs were estimated using Eq. (6) and the results are shown in Table 8.

$$E_f = E_p V_p + E_m V_m \tag{6}$$

The effective moduli of the NR matrix (E_m) and the reinforcing particle (E_p), along with the volume fractions of the particulate filler (V_p) and NR matrix (V_m) obtained from TGA results, were used in the calculations. For the modulus values at 100% strain, the effective modulus of GNPs was directly estimated from the slopes of the stress–strain lines in Fig. 7. The E_f values of the GNP-filled NR samples, calculated using the rule of mixture model (Eq. 6), are presented in Table 8. It is observed that the E_f of G5-filled NR exhibited the highest value, followed by G15 and G25. The E_f values of hybrid GNP-NR samples consistently fall between those of the single GNP-filled NR samples.

Considering the influence of filler orientation, a modified rule of mixtures, as reported in previous studies [37], was applied. This model incorporates factors such as the Krenchel orientation factor (η_0), which depends on filler orientation under applied stress. Values of η_0 were determined in the literature with respective values of 0.825, 0.725, and 0.670 for G5, G15, and G25, respectively [3]. These values decrease with increasing GNP size, suggesting lower orientation due to loops and folds in larger particles. For hybrid GNPs, average orientation factors were calculated based on combinations of individual GNPs in the hybrid systems, resulting in values of 0.775, 0.748, and 0.698 for G5/G15, G5/G25, and G15/G25, respectively. The calculated effective modulus (E_{eff}) of GNPs, using Eq. (8)

$$E_f = E_{eff} V_f \eta_0 \eta_l + E_m V_m \tag{7}$$

$$E_{eff} = \frac{E_f - E_m V_m}{V_f \eta_0 \eta_l} \tag{8}$$

Table 6 Mechanical properties of unfilled and GNP-filled NR

Samples/Properties	E_{100} (MPa)	σ (MPa)	U (%)
NR	1.2 ± 0.1	25.9 ± 2.6	880 ± 10
G5	3.7 ± 0.4	22.9 ± 1.0	520 ± 27
G15	3.2 ± 0.1	21.7 ± 1.1	590 ± 29
G25	2.8 ± 0.2	15.9 ± 1.9	600 ± 34
G5/G15	3.3 ± 0.2	28.9 ± 2.5	630 ± 27
G5/G25	3.1 ± 0.1	28.1 ± 2.2	660 ± 28
G15/G25	2.9 ± 0.1	25.8 ± 1.7	690 ± 35

*E_{100} is a modulus at 100% strain, σ is tensile strength, and U is an ultimate strain

Table 7 Comparison of the modulus at 100% strain of NR filled by different fillers

Fillers	Modulus at 100% strain (MPa)	References
G5	3.7 ± 0.4	Recent study
G15	3.2 ± 0.1	Recent study
G25	2.8 ± 0.2	Recent study
G5/G15	3.3 ± 0.2	Recent study
G5/G25	3.1 ± 0.1	Recent study
G15/G25	2.9 ± 0.1	Recent study
Carbon black	1.0	[3]
Precipitated Silica	1.1	[34]
Fumed silica	1.2	[34]
Silica (2 phr)/ Carbon black (12 phr)	2.0	[35]
$CaCO_3$	1.1	[36]
Nanoclay (5phr)/$CaCO_3$ (10 phr)	2.2	[36]

Table 8 Modulus at 100% strain of all GNP-filled NR

Properties/ Samples	E_{100} (MPa)	E_f (MPa)	η_0	E_{eff} (MPa)
G5	3.7 ± 0.4	41.3 ± 3.2	0.825	50.1 ± 3.4
G15	3.2 ± 0.1	35.5 ± 1.3	0.725	49.0 ± 1.6
G25	2.8 ± 0.2	28.8 ± 2.8	0.670	43.0 ± 3.8
G5/G15	3.3 ± 0.2	38.2 ± 2.9	0.775	49.3 ± 1.0
G5/G25	3.1 ± 0.1	36.0 ± 1.6	0.748	48.2 ± 2.0
G15/G25	2.9 ± 0.1	30.9 ± 1.4	0.698	44.3 ± 1.7

*The analysis includes the modulus of GNP-filled NR at 100% strain (E_{100}), the modulus of GNP calculated using the rule of mixture under iso-stress conditions (E_f), the Krenchel orientation factor determined by Li et al. [3] (η_0). Equation (8) was used to determine the effective elastic modulus of GNP (E_{eff}). E_{100} of unfilled NR was used as an effective modulus of the matrix. The value of 1.2 was used for the calculation

The effective modulus (E_{eff}) represents the modulus of GNPs. η_1 denotes the length distribution factor used as 1 in this research. η_0 represents the Krenchel orientation factor that considers filler orientation under applied stress [37]. The calculated values of E_{eff} of GNPs in GNP-filled NR samples range between 43 and 50 MPa, as demonstrated in Table 8. The effective modulus of G5 in G5-filled NR exhibits the highest value and is consistent with expectations. As anticipated, the effective modulus of hybrid GNPs falls between the values of the individual GNPs they comprise.

Comparing these results to Young's modulus of monolayer graphene, which is around 1 TPa, illustrates a significant reduction, indicating relatively ineffective stress transfer from the low stiffness NR matrix to GNPs, which could be due to the poor dispersion of GNPs in the NR matrix, leading to weak interactions and suboptimal stress transfer, highlighting challenges in harnessing the reinforcement potential of GNPs in low-modulus materials like NR.

Ultimate properties Figure 6(a) and Table 6 provide a comparison of the tensile properties of the samples. In all cases, especially in single GNP-filled NR samples, the elongation at break decreased upon adding GNPs, indicating the brittle behaviour of GNP-filled NR. Poor dispersion, particularly in single GNP systems, resulted in stress concentrators, leading to a larger decrease in elongation at break. The elongation at break of G5-filled NR is approximately 70% less than that of the unfilled NR. Conversely, hybrid GNPs exhibited improved dispersion, reducing the agglutination of NGP particles and enhancing the interfacial interaction with NR and stress transfer efficiency. Thus, hybrid GNP-filled NR samples had higher elongation at break than single GNP-filled NR.

NR inherently exhibits high tensile strength owing to its inherent ability to crystallise under tension, thereby acting as a self-reinforcing filler. Therefore, the addition of GNP particles did not markedly enhance its tensile strength. Substantial decreases in tensile strength were noted with the addition of single GNPs (around 60% for G25-filled NR), whereas hybrid GNPs exhibited more preserved strength. This decrease suggests poor dispersion of GNP particles and inadequate interfacial bonding between GNP and the NR matrix, resulting in decreased tensile strength in single GNP-filled NR. Conversely, the addition of hybrid GNP fillers tended to improve tensile strength. The tensile strength of unfilled NR increased by 12% after adding hybrid GNPs between G5 and G15. These findings underscore the superior performance of hybrid systems over single systems.

Comparing the effects of different GNP sizes on tensile properties revealed that smaller particles, such as G5, improved the most mechanical properties due to their higher number of dispersed particles and greater surface area. However, the elongation at break decreased with decreasing GNP particle size, reflecting the constrained mobility of polymer chains by smaller GNPs. Contrary to some previous findings by Khanx et al. [38] and Chatterjee et al. [39], larger GNPs, like G25, did not exhibit superior reinforcing abilities due to poor dispersion in the NR matrix despite their higher aspect ratio. This underscores the importance of dispersion and interfacial interaction between GNP and the NR matrix, which is enhanced with greater interfacial area. Comparison between single and hybrid GNP-filled demonstrated that hybrid GNPs, benefiting from better dispersion and irregular sizes, displayed higher tensile strength and failure strains due to more efficient stress transfer. Within the hybrid GNP-filled NR samples, those incorporating G5 and G15 exhibited the highest tensile strength and lowest elongation at break, indicating superior interfacial bonding and stress transfer efficiency.

Shore a hardness Figure 8 illustrates that incorporating GNPs into NR led to an increase in hardness across all samples. This enhancement is primarily due to the reduced plasticity and elasticity resulting from the introduction of rigid GNPs, which imparted greater rigidity to the material. The observed increase in hardness can be ascribed to how the

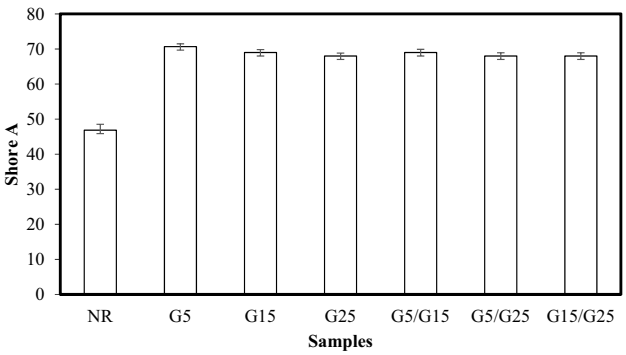

Fig. 8 Hardness (Shore A) of unfilled and GNP-filled NR

distribution of GNP fillers limits the mobility of elastomer chains. NR reinforced with the smallest particles, G5-filled NR, shows higher hardness than NR filled with larger GNPs due to their increased contact areas with the NR matrix. Similar to other mechanical properties, the hardness values of hybrid GNP-filled NR fell between those of each single GNP-filled NR, consistent with the principles of the rule of mixture, where hardness correlates with the elastic modulus.

The hardness results align with the modulus values at 100% strain (E_{100}) obtained for all GNP-filled NR, as shown in Table 8. While interfacial adhesion alone would suggest that NR reinforced with hybrid GNPs should exhibit higher hardness than those with a single filler, the results revealed the opposite trend. This can be explained by the fact that hardness is a property measured under low-strain conditions, where the minimal deformation causing separation at the NR-filler interface has little impact on interfacial bonding, as noted by Fu et al. [40].

Thermal and thermo-mechanical properties

Dynamic mechanical analysis The reinforcing effectiveness of GNP of different sizes in GNP-filled NR was assessed and compared using DMA. Figure 9(a) shows the temperature-dependent storage modulus (E'), whereas Fig. 9(b) presents the loss tangent (tan δ) of unfilled and GNP-filled NR. These dynamic properties are closely related to energy distribution within materials, influenced by filler dispersion, volume fraction, size, and load transfer [41]. Below -60 °C, all samples were in a glassy state, with storage moduli around 2 GPa for unfilled NR and at least 4.0 GPa for GNP-filled NR. This increase in glassy moduli was attributed to adding

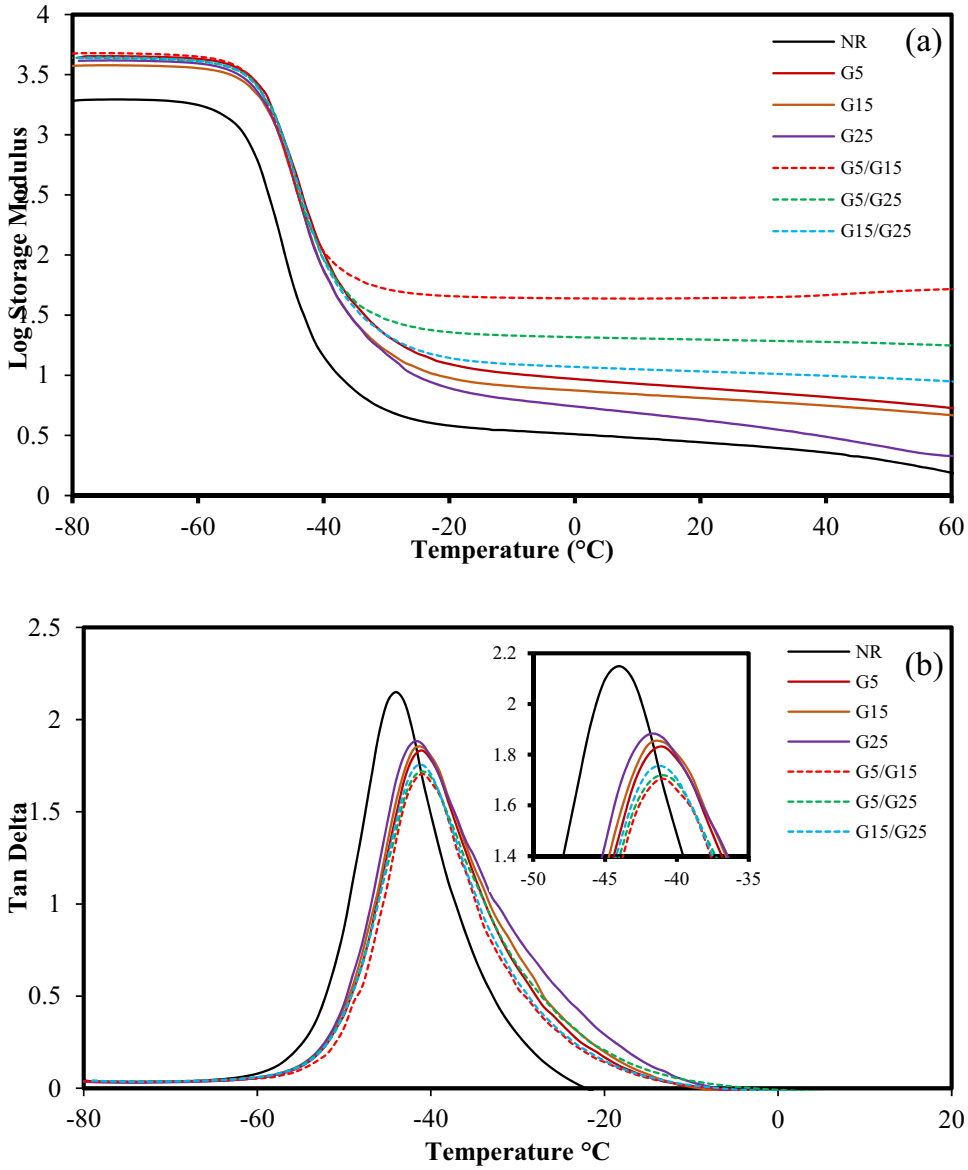

Fig. 9 Log storage modulus (**a**) and tan delta (**b**) of unfilled and GNP-filled NR as a function of temperature

GNPs with high elastic modulus, typically around 1 TPa, for defect-free single graphene layers [15]. A substantial decrease in storage modulus was observed around -40 °C, corresponding with the primary energy dissipation at Tg of GNP-filled NR. This phenomenon, accompanied by a peak in the loss tangent, resulted from cooperative movements of long-chain sequences. Above Tg, the storage modulus plateaued, indicating the rubbery state, with interactions between fillers and the NR matrix influencing composite properties [41].

The reinforcing efficiency of GNPs varied, with smaller particles yielding higher storage moduli, especially evident in the rubbery region. Hybrid GNPs exhibited superior reinforcing effects, likely due to better dispersion and increased surface area. The interaction between NR and GNPs constrained polymer chain mobility, evidenced by shifts in the tan δ peaks to higher temperatures, indicating higher T_g values and reduced polymer chain dynamics [30, 41]. Among the single GNP-filled NR samples, G5-filled NR exhibited the highest T_g and the least intense maximum tan δ peak, as indicated in Table 9, suggesting enhanced interactions between GNP and the NR matrix and greater polymer chain confinement. The hybrid GNPs further elevated T_g and diminished the intensity of the tan δ peak, underscoring enhanced interfacial interactions with the NR matrix compared to single GNPs. These findings suggest that hybrid GNPs, with better dispersion and enhanced reinforcing ability, offer improved dynamic properties in GNP-filled NR.

Differential scanning calorimetry DSC is a widely used technique for examining the thermal behaviour of polymer materials, including determining the Tg of unfilled NR and GNP-filled NR in this study. Figure 10(a) displays the second DSC heating scan of the unfilled and GNP-filled NR samples, revealing distinct glass transitions. The T_g values derived from the DSC curves are summarised in Fig. 10(b). A slight increase in Tg was observed with the addition of single GNPs. Notably, the increase was more pronounced for the hybrid GNP-filled NR, highlighting enhanced interfacial interactions between GNP and the NR matrix. This

Table 9 Tan δ peaks and T_g of unfilled and GNP-filled NR

Sample/Properties	Tan $(\delta)_{max}$	T_g (°C)	Reduction of tan δ_{max} (%)
NR	2.15	-44.1 ± 0.1	-
G5	1.83	-41.3 ± 0.2	14.88
G15	1.85	-41.4 ± 0.2	13.95
G25	1.88	-41.7 ± 0.4	12.56
G5/G15	1.71	-39.9 ± 0.3	20.47
G5/G25	1.72	-41.1 ± 0.2	20.00
G15/G25	1.75	-41.3 ± 0.1	18.60

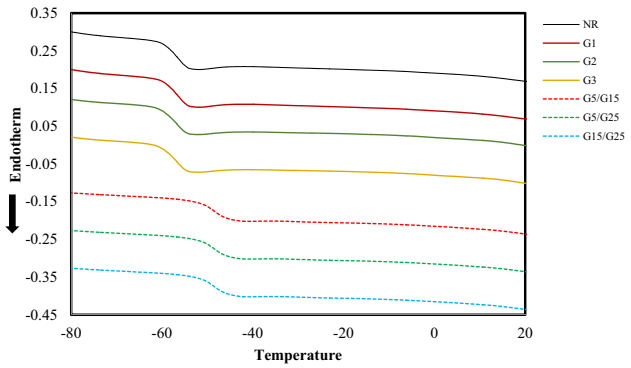

Fig. 10 DSC from the second heating scan

led to a more significant polymer chain mobility restriction in NR and a reduction in free volume. These results are attributed to the superior dispersion of hybrid GNPs, which offer larger interaction surfaces with the NR matrix, consistent with earlier findings in this study (Table 10).

Notably, the T_g values measured by DMA and DSC exhibited some discrepancies. This could be attributed to variations in methodology and heating/cooling rates employed in this study. However, despite this variance, both techniques consistently demonstrated the same trend in the T_g values of the unfilled and all GNP-filled NR samples.

Thermogravimetric analysis Thermogravimetric analysis (TGA) was utilised to examine the thermal stability of the NR matrix and GNP-filled NR. Figure 11(a) illustrates the weight loss versus temperature curves, while Fig. 11(b) shows the decomposition rate of the unfilled and GNO-filled NR samples. The results indicate that at lower temperatures, the thermal stability of NR was not significantly improved by the incorporation of GNPs. However, at the temperature above 400 °C, all GNP-filled NR samples showed a reduced maximum thermal decomposition rate compared to unfilled NR. Additionally, there is an apparent increase in residual char yield at the end of the test, primarily attributed to the presence of added GNPs remaining after the volatilisation of the NR matrix.

The thermal degradation behaviour of all GNP-filled NR samples exhibited a similar one-step weight loss pattern. The unfilled NR began to thermally decompose at around 370 °C, with substantial weight loss occurring during pyrolysis until it ended at around 440 °C. Table 11 summarises the different decomposition temperatures of unfilled and GNP-filled NR samples obtained from the TGA curves. Notably, the onset decomposition temperatures (T_0) of all GNP-filled NR were lower than that of unfilled NR, indicating that GNPs facilitate earlier decomposition due to enhanced heat transfer within the GNP-filled NR. This indicates that incorporating GNPs does not enhance the degradation

Table 10 Glass transition temperature (Tg) of unfilled and GNP-filled NR

Sample	G5	G15	G25	G5/G15	G5/G25	G15/G25
T_g (°)	-61.4 ± 0.1	-60.9 ± 0.2	-61.0 ± 0.3	-52.2 ± 0.2	-52.7 ± 0.4	-53.0 ± 0.2

temperature of the NR matrix due to enhanced heat transfer within the GNP-filled NR.

At lower temperatures below approximately 390 °C, shown in Fig. 11(b), there was an observed increase in the thermal degradation rate, accompanied by a decrease in the onset temperature of thermal degradation (T_0) for all GNP-filled NR samples. These phenomena contribute to the high specific surface areas and thermal conductivity of GNPs that accelerate heat transfer of GNP-filled NR [42]. However, all GNP-filled NR exhibited slower weight loss at higher temperatures than unfilled NR, likely because of the tortuosity effect. This effect slows the release of volatile degradation materials and promotes char formation [43]. During thermal degradation, GNPs may hinder the diffusion of small gas molecules, and the oxygen supply may be obstructed by charred layers formed on the NR matrix surfaces [21]. Overall, some beneficial effects on the thermal behaviour of the NR are observed upon adding GNPs, including a reduction in the thermal degradation rate at higher temperatures.

The thermal degradation rate of GNP-filled NR varies based on the lateral diameter of GNPs. Smaller GNPs show accelerated thermal degradation at lower temperatures but slower degradation at higher temperatures, owing to their enhanced heat transfer efficiency and improved dispersibility and interfacial adhesion. Compared with NR reinforced by hybrid GNPs, NR reinforced by single GNPs exhibited a lower degradation rate at lower temperatures but a higher rate at higher temperatures. This difference can be attributed

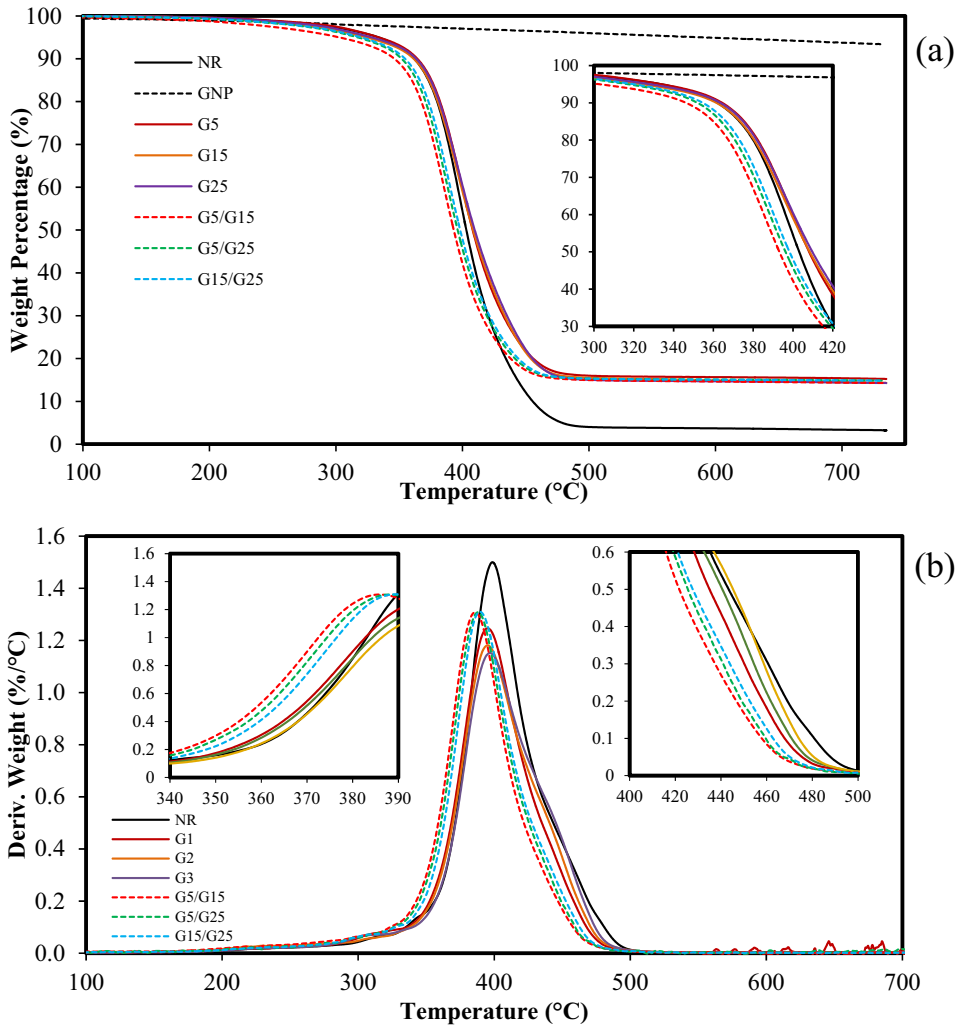

Fig. 11 Weight loss (**a**) and the resulting weight (**b**) obtained from TGA results for unfilled and GNP-filled NR

Table 11 Thermal degradation temperatures of unfilled and GNP-filled NR determined by the TGA results

Samples	Onset decomposition temperatures/ T_0 (°C)	Fastest decomposition temperature/ T_f (°C)	End set decomposition temperature /T_e (°C)
NR	367 ± 2	399 ± 1	437 ± 4
G5	359 ± 3	397 ± 1	439 ± 1
G15	360 ± 2	395 ± 1	436 ± 1
G25	361 ± 4	393 ± 6	428 ± 9
G5/G15	346 ± 2	388 ± 1	428 ± 4
G5/G25	352 ± 2	387 ± 1	430 ± 1
G15/G25	354 ± 5	388 ± 2	428 ± 5

to the enhanced dispersion of GNPs in hybrid form within the NR matrix, facilitating better heat transfer at lower temperatures. At the same time, at higher temperatures, the mobility of volatiles is limited; consequently, the thermal stability observed in the NR matrix was improved. Comparison with hybrid GNP-filled NR reveals that the degradation rate of single GNP-filled NR was lower at lower temperatures. Conversely, at higher temperatures, it was higher. This difference is likely attributed to the improved dispersion of hybrid GNPs within the NR matrix. The enhanced dispersion of hybrid GNPs within the NR matrix facilitates more efficient heat transfer at lower temperatures. Additionally, it effectively restricts the mobility of volatiles at higher temperatures, thereby contributing to the overall improvement in the thermal stability of the NR matrix.

Electrical properties of GNP-filled NR

The influence of GNP particle size and hybrid systems on the electrical properties of GNP-filled NR was examined. Figure 12 shows the electrical conductivity plotted against frequency, and Table 12 lists the electrical conductivity values at 10^6 Hz. As expected, incorporating GNPs enhanced the electrical conductivity of the NR matrix across all GNP-filled NR samples, attributable to the superior conductivity of GNP. Figure 12 demonstrates that as the frequency increases, there is a corresponding increase in electrical conductivity. This phenomenon aligns with the principle that materials exhibit decreased electrical resistance at higher test frequencies, enabling more efficient electron conduction across the GNP-NR interfaces through frequency-induced electron hopping [44].

Consistent with expectations, the electrical conductivity increased with larger lateral sizes of GNPs, from 5 µm to 25 µm. Larger particulate fillers facilitate the formation of conductive networks due to less dispersion, thereby enhancing the electrical conductivity of GNP-filled NR. Conversely, smaller GNPs, well-dispersed within the NR matrix, reduced the formation of conductive electrical networks, resulting in lower electrical conductivity than larger GNPs.

The electrical conductivity of GNP-filled NR is directly influenced by the distance between neighbouring GNPs at low frequencies [44]. As shown in Fig. 12, G25-filled NR exhibited considerably higher electrical conductivity at low frequencies than G5- and G15-filled NR, suggesting shorter distances between GNP particles within the NR matrix. This observation is supported by SEM micrographs of fracture surfaces shown in Fig. 13, where an increase in GNP size corresponded to a reduction in the spacing between GNP plates. Therefore, the electrical conductivity results align with findings from other characterisation methods in this study, indicating that the GNP-filled NR with the largest particles exhibited the lowest dispersion within the NR matrix.

The electrical conductivity of hybrid GNP-filled NR samples surprisingly surpassed that of some NR reinforced

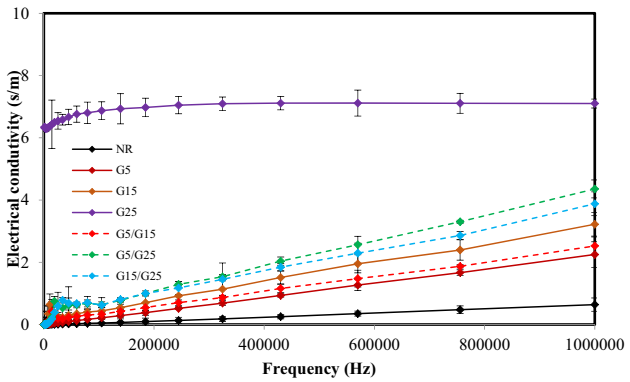

Fig. 12 (**a**) Electrical conductivity plotted against frequency

Table 12 Electrical conductivity of unfilled and GNP-filled NR at 10^6 Hz

Samples	Electrical conductivity (S/m)	Increase (%)
NR	0.64 ± 0.2	-
G5	2.10 ± 0.4	228 ± 64
G15	3.22 ± 0.4	403 ± 59
G25	7.10 ± 0.1	1008 ± 22
G5/G15	2.93 ± 0.4	357 ± 55
G5/G25	4.35 ± 0.3	579 ± 45
G15/G25	3.88 ± 0.4	505 ± 59

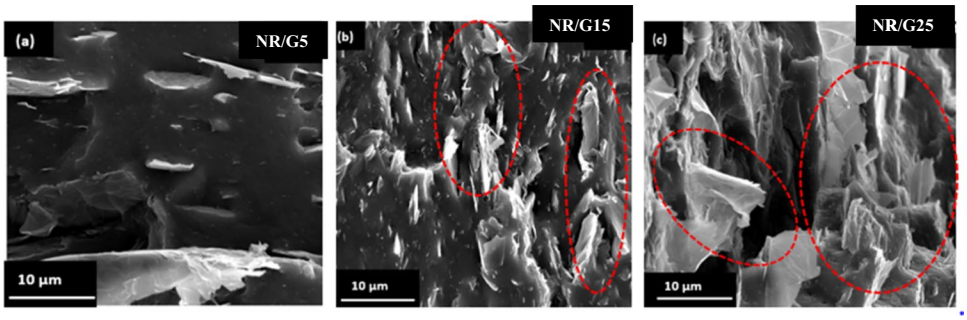

Fig. 13 SEM images of tensile broken surfaces of GNP-filled NR (**a**) G5, (**b**) G15 and (**c**) G25

with smaller single GNPs. Usually, dispersion being crucial, one might expect lower electrical conductivity in NR with hybrid GNPs compared to NR with single GNPs. Li and Kim [45], however, suggested that the electrical conductivity of composite materials can be influenced by the filler thickness. The conductivity will increase linearly when the thickness of the filler decreases. The possibility of improved conductivity with a hybrid filler arises from reduced contact resistance between particles of different fillers, resulting in less agglomeration within the composite material and a thinner polymer layer between different GNPs [46]. These factors contribute to enhanced electrical properties compared to systems with single fillers. The electrical conductivity of unfilled and GNP-filled NR samples at a frequency of 10^6 Hz is presented in Table 12. The electrical conductivity of the NR matrix was increased by approximately 1000% after the addition of the largest GNP (G25), whereas the electrical conductivity of the NR matrix could be enhanced by only around 200% and 600% by the addition of the smallest GNP (G5) and hybrid GNPs.

In conclusion, the electrical conductivity of GNP-filled NR in this study was mainly influenced by the size and aspect ratio of the GNP, with larger GNP resulting in higher conductivity. Additionally, filler geometry, such as thickness, played a role, with fewer graphene layers leading to higher conductivity. However, the study found that GNP size had a much greater impact on electrical conductivity than GNP thickness.

Conclusion

In this research, GNP-filled NR were prepared using a mini-internal mixer operated in Banbury mode for dispersion. Incorporating GNPs into NR resulted in notable enhancements in thermal and electrical properties, alongside partial improvements in mechanical properties. While GNPs contributed to enhancements in modulus, hardness, and strain-induced crystallisation of the NR matrix, they also led to reduced elongation at break due to constrained polymer chain mobility. Interestingly, the addition of single GNPs did not increase the tensile strength of NR, indicating inefficient stress transfer at the interfacial areas between NR and GNP. Moreover, the effective modulus values of GNPs in GNP-filled NR samples were substantially lower than that of a single graphene layer, highlighting the inefficiency of stress transfer.

A comprehensive comparative analysis encompassed three different GNP particle sizes (G5, G15 and G25) and three hybrid GNP systems (G5/G15, G5/G25 and G15/G25). The findings revealed several key conclusions. Smaller GNP particle sizes demonstrated superior mechanical properties compared to larger GNPs, attributed to a greater number of dispersed particles with larger surface areas facilitating stronger interfacial bonding with NR. The modulus at 100% strain, tensile strength and hardness of G5-filled NR was around 30%, 45% and 5%, respectively, higher than that of G25-filled NR. Increasing GNP lateral diameters resulted in reduced enhancements in thermal properties, as larger particles exerted less influence on polymer chain mobility. Smaller GNP sizes conferred higher thermal stability to GNP-filled NR, reducing the thermal degradation rate. Larger GNP particle sizes promoted higher electrical conductivity due to increased surface area and aggregate network formation caused by lower dispersion. The electrical conductivity of the NR matrix was increased by around 1,000% after adding G25. NR/GNP hybrid systems exhibited superior mechanical and thermal properties compared to NR/single GNP nanocomposites, attributed to better dispersion and irregular sizes leading to more efficient stress transfer. However, lower electrical conductivity was observed in the hybrid systems.

These findings provide valuable insights into optimising the properties of GNP-filled NR for diverse applications. Undertaking additional testing or simulations to assess the long-term stability and durability of GNP-filled NR is recommended, as these would significantly enhance their practical usability across different fields. These efforts would offer valuable insights into how these nanocomposites perform over extended periods, ensuring they are reliable and effective in real-world applications.

Acknowledgements This work was supported by the Department of Materials and Metallurgical Engineering, Faculty of Engineering, Rajamangala University of Technology Thanyaburi. We would also like to thank the reviewers for their valuable comments.

Funding Institute of Research and Development, Rajamangala University of Technology Thanyaburi.

Data Availability Data is contained within the article.

Declarations

Ethical Approval Not Applicable.

Conflicts of Interest The authors declare no conflict of interest.

References

1. Rashid AA, Yahya SR (2014) In: Natural rubber materials, volume 2: composites and nanocomposites: mechanical properties of natural rubber composites filled with macro- and nanofillers. The Royal Society of Chemistry, Cambridge
2. Chan CH, Joy J, Maria J (2014) Natural rubber materials, volume 2: composites and nanocomposites: natural rubber-based composites and nanocomposites : state of the art, new challenges and opportunities. The Royal Society of Chemistry, Cambridge
3. Li S, Li Z, Burnett TL, Slater TJA, Hashimoto T, Young RJ (2017) Nanocomposites of graphene nanoplatelets in natural rubber: microstructure and mechanisms of reinforcement. J Mater Sci 52(2017):9558–9572. https://doi.org/10.1007/s10853-017-1144-0
4. Basu D, Das A, Stöckelhuber KW, Wagenknecht U, Heinrich G (2014) Advances in layered double hydroxide (LDH)-based elastomer composites. Prog Polym Sci 39:594–626. https://doi.org/10.1016/j.progpolymsci.2013.07.011
5. Novoselov AAFKS, Geim AK, Morozov SV, Jiang DE, Zhang Y, Dubonos SV, Grigorieva V (2004) Electric field effect in atomically thin carbon films. Science 306(5696):666–669. https://doi.org/10.1126/science.1102896
6. Geim AK, Novoselov KS (2007) The rise of graphene. Nat Mater 6:183–191. https://doi.org/10.1038/nmat1849
7. Novoselov KS, Geim AK, Morozov SV, Jiang D, Katsnelson MI, Grigorieva IV, Dubonos SV, Firsov AA (2005) Two-dimensional gas of massless Dirac fermions in graphene. Nature 438:197–200. https://doi.org/10.1038/nature04233
8. El-Khawas EH, Azab AA, Mansour AM (2020) Structural, magnetic and dielectric properties of reduced graphene oxide/La0. 9Bi0. 1FeO3 nanocomposites. Mater Chem Phys 241:122335. https://doi.org/10.1016/j.matchemphys.2019.122335
9. Young RJ, Kinloch IA (2013) Graphene and graphene-based nanocomposites. Nanostructures through Chem. https://doi.org/10.1039/9781849734844-00145
10. Young RJ, Kinloch IA, Gong L, Novoselov KS (2012) The mechanics of graphene nanocomposites: A review. Compos Sci Technol 72:1459–1476. https://doi.org/10.1016/j.compscitech.2012.05.005
11. Young RJ, Liu M (2016) The microstructure of a graphene-reinforced tennis racquet. J Mater Sci 51:3861–3867. https://doi.org/10.1007/s10853-015-9705-6
12. Azira AA, Kamal MM, Rusop M (2016) Reinforcement of graphene in natural rubber nanocomposite. AIP Conf Proc 173:1733. https://doi.org/10.1063/1.4948821
13. Papageorgiou DG, Kinloch IA, Young RJ (2015) Graphene/elastomer nanocomposites Carbon N Y 95:460–484. https://doi.org/10.1016/j.carbon.2015.08.055
14. Wijerathne D, Gong Y, Afroj S, Karim N, Abeykoon C (2023) Mechanical and thermal properties of graphene nanoplatelets-reinforced recycled polycarbonate composites. Int J Light Mater Manuf 6:117–128. https://doi.org/10.1016/j.ijlmm.2022.09.001
15. xGnP® Graphene Nanoplatelets – Grade M (2012) XG Sciences Inc., Lansing, Michigan. http://www.xgsciences.com. Accessed 19 Feb 2024
16. Müller MT, Hilarius K, Liebscher M, Lellinger D, Alig I, Pötschke P (2017) Effect of graphite nanoplate morphology on the dispersion and physical properties of polycarbonate based composites. Materials 10(5):545. https://doi.org/10.3390/ma10050545
17. Um JG, Jun YS, Alhumade H, Krithivasan H, Lui G, Yu A (2018) Investigation of the size effect of graphene nano-platelets (GnPs) on the anti-corrosion performance of polyurethane/GnP composites. R Soc Chem 8:17091–17100. https://doi.org/10.1039/c8ra02087f
18. Wall M (2011) The Raman spectroscopy of graphene and the determination of layer thickness. Thermo Fisher Scientific, Madison, Wisconsin. https://tools.thermofisher.com. Accessed 19 Feb 2024
19. Shearer CJ, Slattery AD, Stapleton AJ, Shapter JG, Gibson CT (2016) Accurate thickness measurement of graphene. Nanotechnology 27:125704–125714. https://doi.org/10.1088/0957-4484/27/12/125704
20. Reich S, Thomen C (2004) Raman spectroscopy of graphite. R Soc 362:2271–2288. https://doi.org/10.1098/sta.2004.1454
21. Prolongo SG, Jiménez-Suárez A, Moriche R, Ureña A (2014) Graphene nanoplatelets thickness and lateral size influence on the morphology and behavior of epoxy composites. Eur Polym J 53:292–301. https://doi.org/10.1016/j.eurpolymj.2014.01.019
22. Raza MA, Westwood AVK, Brown AP, C. (2012) Stirling, Texture, transport and mechanical properties of graphite nanoplatelet/silicone composites produced by three roll mill. Compos Sci Technol 72:467–475. https://doi.org/10.1016/j.compscitech.2011.12.010
23. Hernández M, del Mar Bernal M, Verdejo R, Ezquerra TA, López-Manchado MA (2012) Overall performance of natural rubber/graphene nanocomposites. Compos Sci Technol 73:40–46. https://doi.org/10.1016/j.compscitech.2012.08.012
24. Chong HM, Hinder SJ, Taylor AC (2016) Graphene nanoplatelet-modified epoxy: effect of aspect ratio and surface functionality on mechanical properties and toughening mechanisms. J Mater Sci 51:8764–8790. https://doi.org/10.1007/s10853-016-0160-9
25. Johns J, Rao V (2008) Characterisation of natural rubber latex/chitosan blends. Int J Polym Anal Charact 13:280–291. https://doi.org/10.1080/10236660802190104
26. Scherrer P (1912) In: Kolloidchemie Ein Lehrbuch. Chemische Technologie in Einzeldarstellungen Bestimmung der inneren Struktur und der Größe von Kolloidteilchen mittels Röntgenstrahlen. Springer, Berlin, Heidelberg
27. Wang F, Drzal LT, Qin Y, Huang Z (2016) Size effect of graphene nanoplatelets on the morphology and mechanical behavior of glass fiber / epoxy composites. J Mater Sci 51:3337–3348. https://doi.org/10.1007/s10853-015-9649-x
28. Dul S, Fambri L, Merlini C, Barra GMO, Bersani M, Vanzetti L, Pegoretti A (2008) Effect of graphene nanoplatelets structure on the properties of acrylonitrile–butadiene–styrene composites. Polym Polym Compos 16:101–113. https://doi.org/10.1002/pc.24645
29. Fröhlich J, Niedermeier W, Luginsland H-D (2005) The effect of filler–filler and filler–elastomer interaction on rubber reinforcement. Compos Part A Appl Sci Manuf 36:449–460. https://doi.org/10.1016/j.compositesa.2004.10.004
30. Zhang C, Dan Y, Peng J, Turng L-S, Sabo R, Clemons C (2014) Thermal and mechanical properties of natural rubber composites reinforced with cellulose nanocrystals from southern pine. Adv Polym Technol 33:21448. https://doi.org/10.1002/adv.21448

31. Ghosh OSN, Gayathri S, Sudhakara P, Misra SK, Jayaramudu J (2017) In. In: Markovic G, PM V (eds) Rubber Nano Blends: Preparation, Characterisation and Applications. Springer Series on Polymer and Composite Materials. Springer, Cham
32. Samsuri AB (2013) In: Natural rubber materials, volume 2: composites and nanocomposites: theory and mechanisms of filler reinforcement in natural rubber. The Royal Society of Chemistry, Cambridge
33. Coleman JN, Khan U, Blau WJ, Gun YK (2006) Small but strong : A review of the mechanical properties of carbon nanotube-polymer composites. Carbon N Y 44:1624–1652. https://doi.org/10.1016/j.carbon.2006.02.038
34. Prasertsri S, Rattanasom N (2012) Fumed and precipitated silica reinforced natural rubber composites prepared from latex system: Mechanical and dynamic properties. Polym Test 31:593–605. https://doi.org/10.1016/j.polymertesting.2012.03.003
35. Leekrajang M, Chutichairattanaphum N, Larpkiattaworn S, Panichpakdee J, Somwongsa P (2020) The effects of silica/carbon black hybrid filler contents on natural rubber composite properties using conventional vulcanization system. J Sci Innov Technol 3(2):13–23
36. Ghari HS, Jalali-Arani A (2016) Nanocomposites based on natural rubber, organoclay and nano-calcium carbonate: Study on the structure, cure behavior, static and dynamic-mechanical properties. Appl Clay Sci 119:348–357
37. Li Z, Young RJ, Wilson NR, Kinloch IA, Vallés C, Li Z (2016) Effect of the orientation of graphene-based nanoplatelets upon the Young's modulus of nanocomposites. Compos Sci Technol 123:125–133. https://doi.org/10.1016/j.compscitech.2015.12.005
38. Khan U, May P, Neill AO, Coleman JN (2010) Development of stiff, strong, yet tough composites by the addition of solvent exfoliated graphene to polyurethane. Carbon N Y 48:4035–4041. https://doi.org/10.1016/j.carbon.2010.07.008
39. Chatterjee S, Nafezarefi F, Tai NH, Schlagenhauf L, Nu FA (2012) Size and synergy effects of nanofiller hybrids including graphene nanoplatelets and carbon nanotubes in mechanical properties of epoxy composites. Carbon N Y 50:5380–5386. https://doi.org/10.1016/j.carbon.2012.07.021
40. Fu SY, Feng XQ, Lauke B, Mai YW (2008) Effects of particle size, particle/matrix interface adhesion and particle loading on mechanical properties of particulate-polymer composites. Compos PartB Eng 39:933–961. https://doi.org/10.1016/j.compositesb.2008.01.002
41. Wu X, Lin TF, Tang ZH, Guo BC, Huang GS (2015) Natural rubber/graphene oxide composites: Effect of sheet size on mechanical properties and straininduced crystallisation behavior. Express Polym Lett 9:672–685. https://doi.org/10.3144/expresspolymlett.2015.63
42. Puglia D, Valentini L, Kenny JM (2003) Analysis of the cure reaction of carbon nanotubes / epoxy resin composites through thermal analysis and raman spectroscopy. Appl Polym Sci 88:452–458. https://doi.org/10.1002/app.11745
43. Wang X, Xing W, Zhang P, Song L, Yang H, Hu Y (2012) Covalent functionalisation of graphene with organosilane and its use as a reinforcement in epoxy composites. Compos Sci Technol 72:737–743. https://doi.org/10.1016/j.compscitech.2012.01.027
44. Ravindran A, Feng C, Huang S, Wang Y, Zhao Z, Yang J (2018) Effects of graphene nanoplatelet size and surface area on the AC electrical conductivity and dielectric constant of epoxy nanocomposites. Polymers (Basel) 10:477–494. https://doi.org/10.3390/polym10050477
45. Li J, Kim J (2007) Percolation threshold of conducting polymer composites containing 3D randomly distributed graphite nanoplatelets. Compos Sci Technol 67:2114–2120. https://doi.org/10.1016/j.compscitech.2006.11.010
46. Perets Y, Aleksandrovych L, Melnychenko M, Lazarenko O, Vovchenko L, Matzui L (2017) The electrical properties of hybrid composites based on multiwall carbon nanotubes with graphite nanoplatelets. Nanoscale Res Lett 12:406. https://doi.org/10.1186/s11671-017-2168-8